NJC

Accepted Manuscript

This is an Accepted Manuscript, which has been through the Royal Society of Chemistry peer review process and has been accepted for publication.

Accepted Manuscripts are published online shortly after acceptance, before technical editing, formatting and proof reading. Using this free service, authors can make their results available to the community, in citable form, before we publish the edited article. We will replace this Accepted Manuscript with the edited and formatted Advance Article as soon as it is available.

You can find more information about Accepted Manuscripts in the author guidelines.

Please note that technical editing may introduce minor changes to the text and/or graphics, which may alter content. The journal's standard Terms & Conditions and the ethical guidelines, outlined in our author and reviewer resource centre, still apply. In no event shall the Royal Society of Chemistry be held responsible for any errors or omissions in this Accepted Manuscript or any consequences arising from the use of any information it contains.

ROYAL SOCIETY OF CHEMISTRY

rsc.li/njc

New Journal of Chemistry

ARTICLE

Synthesis, Structural Characterization and Computational Study of a Novel Amino Chalcone: a Potential Nonlinear Optical Material

Received 00th January 20xx,
Accepted 00th January 20xx

DOI: 10.1039/x0xx00000x

www.rsc.org/

Leonardo R. Almeida,[a] Murilo M. Anjos,[b] Gabriela C. Ribeiro,[a] Clodoaldo Valverde[a,c], Daniel F. S. Machado,[d] Guilherme R. Oliveira,*[b] Hamilton B. Napolitano*[a] and Heibbe. C. B. de Oliveira*[d]

Abstract The interest for novel chalcone-based materials in nonlinear optics is dependent on strong second harmonic generation in organic systems. Chalcones are α,β-unsaturated ketones that can be easily obtained by Claisen-Schmidt condensation between ketones and aromatic aldehydes. A new 2-amino-chalcone was synthesized and its crystal molecular structure was elucidated using single crystal X-ray diffraction technique. This compound, $C_{15}H_{12}BrNO_2$, crystallizes in monoclinic centrosymmetric space group C2/c with cell parameters a = 29.47(7) Å; b = 6.97(5) Å, c = 13.59(1) Å, β = 112.52(6)° and V = 2581.2(2) Å^3. In addition to crystal structure, the analysis of Hirshfeld surfaces indicates the presence of hydrogen bonds of types N–H···O, O–H···O that stabilize two independent centrosymmetric dimer, and also indicates the presence of π-π stacking interaction that stabilizes a supramolecular trimeric system. Being a push-pull chromophore we investigated the NLO properties of the 2-amino-chalcone asymmetric unit using the supermolecule approach in combination with an iterative electrostatic polarization scheme. The calculations were performed using CAM-B3LYP/6-311+G(d) level of theory for both dynamic and static situations. In the presence of the embedding charges, the γ value is increased by 20% for the dynamic calculation but only 8% for the static limit. In contrast to the crystal form, when in solution the 2-amino-chalcone lacks inversion center so that second order NLO properties do not vanish. Following this idea we computed the NLO properties using the implicit solvation approach IEF-PCM. The solvent effect on NLO properties was to augment its values as the solvent polarity increases. We obtained for the in-crystal and in DMSO 2-amino-chalcone, γ(-2ω;ω,ω,0) = 144.12×10^{-36} esu and 260.163×10^{-36} esu, respectively and therefore an interesting material for third order NLO applications.

Introduction

The interest for novel organic-based materials in nonlinear optics (NLO) arose in the 1970's when Davydov and co-workers reported a strong second harmonic generation (SHG) in organic systems.[1] The relative ease of synthesis, manipulation and possibly higher NLO efficiencies that organic structures provide for technological applications have raised much attention, and still today several researches are devoted to the rational synthesis of chromophores to optimize a given NLO property.[2,3] These chromophores are generally donor-acceptor π-electron systems (D-A) which possess a conjugated path or bridge, giving rise to an asymmetric electron's density distribution. Indeed, structure-property relationships exert acute influence on NLO properties of organic-based materials where some structural parameters such as D-A strength, D-A relative position and conjugation length,[4,5] can modulate a desired property. For example, molecular asymmetry, i.e. acentricity, plays an important role for second and third-order nonlinearity. Theoretical investigations have been playing an invaluable role in helping experimental studies to understand the microscopic origin of the molecular NLO responses and designing new chromophores with large NLO properties, that is, tuning the molecular parameters that give the optimal desired property. For instance, Oliveira and co-workers have investigated the D-A effects on the first hyperpolarizability (static and dynamic) of azo-enaminones derivatives using HF and MP2 approximations and observed that this property increases as a function of the donor group strength.[6–8] As a contrasting example of how important theoretical calculations are, Jacquemin demonstrated through MP2 and HF approximations, that polyaminoborane and polyiminoborane oligomers are poor candidates for NLO applications.[9]

Among organic materials, those of chalcones derivatives have proven to be potential candidates for NLO applications as reported by Agrinskaya *et al.*,[10] who obtained poly-crystalline chalcone materials that exhibit a high nonlinear activity. In

[a] Campus de Ciências Exatas e Tecnológicas, Universidade Estadual de Goiás, Caixa Postal 459, 75001-970, Anápolis, GO, Brazil.
[b] Instituto de Química, Universidade Federal de Goiás, Caixa Postal 131, Campus Samambaia, 74001-970, Goiânia, GO, Brazil.
[c] Universidade Paulista, 74845-090 and Escola Superior Associada de Goiânia, 74840-090, Goiânia, GO, Brazil.
[d] Laboratório de Estrutura Eletrônica e Dinâmica Molecular (LEEDMOL), Instituto de Química, Universidade de Brasilia, Caixa Postal 4478, 70904-970, Brasilia, DF, Brazil.

Electronic Supplementary Information (ESI) available: [details of any supplementary information available should be included here]. See DOI: 10.1039/x0xx00000x

their work, the measured macroscopic nonlinear susceptibility χ2 was compared with the calculated values of β, the first-order hyperpolarizability tensor. Ganapayya *et al.*, in turn, synthesized and crystallized another chalcone derivative with SHG efficiency comparable to that of urea,[11] and Kumar *et al.* obtained another chalcone derivative with optical transparency in the visible region, useful for NLO device applications.[4]

Chalcones are α,β-unsaturated ketones that can be easily obtained by Claisen-Schmidt condensation between ketones and aromatic aldehydes under either acidic or basic conditions.[12,13] The class is reported to have a broad spectrum of biological activities such as: anti-microbial,[14] anti-inflammatory,[15] cytotoxic,[16] anticancer,[17] anti-leishmanial,[18] etc. In addition to its biological importance, under appropriate reaction conditions, 2-amino-chalcones have been used as precursors of quinoliniques derivatives, azo analogues of flavanones and flavones in organic synthesis.[19,20] Based on our interest in the chemistry of chalcones and their applications,[21–23] the compound (E)-1-(2-aminophenyl)-3-(5-bromo-2-hydroxyphenyl)prop-2-en-1-one (named here as 2-amino-chalcone), $C_{15}H_{12}BrNO_2$ (Figure 1), was synthesized and its crystallographic structure was elucidated using single crystal x-ray diffraction technique. The highly unsaturated 2-amino-chalcone exhibits mesomeric effects, polarizing the molecule due to the presence of bromine (acceptor) and amino (donor) substituents on the double bonds across the molecule. It turns out that the 2-amino-chalcone system shows the so-called push-pull or donor-acceptor molecular systems that induce asymmetric polarization, enhancing the quadratic NLO properties. The mesomeric effect entails delocalization of π-electrons, polarizing the olefinic carbons and thus stabilizing the polarized structure. To account for this asymmetric electronic distribution, we have performed theoretical calculations based on the Kohn-Sham Density Functional Theory (DFT)[24,25] aiming to evaluate the non-linear optical properties for the aforementioned compound. In fact, the polarizabilities and higher orders (second and third) hyperpolarizabilities characterize the degree of distortion of the molecular electron cloud resulting from the application of an external electric field. They are dynamic electrical properties related to optical phenomena, such as absorption and refraction and also nonlinear optical phenomena and we will consider both static and dynamic (frequency-dependent) approach to compute the electrical properties. Dynamic calculations take into account frequency dispersion contributions which are reported to give more accurate NLO properties.[7,26]

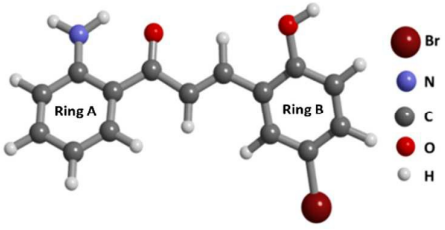

Figure 1. Structural formula of 2-amino-chalcone ($C_{15}H_{12}BrNO_2$).

The determination of these electrical properties is essential, among others, for the better understanding of the dispersion forces and intermolecular long-range induction. In this work, we have used a supermolecular approach in an iterative electrostatic scheme to determine the dipole moment μ, average linear polarizability <α>, first hyperpolarizability β, and second hyperpolarizability γ of the amino chalcone within the crystalline environment. Fonseca and co-workers have calculated μ, <α> and β using this supermolecular approach of embedding charges of L-arginine phosphate monohydrate using the MP2/6-311+G(d) level of theory.[27] The iteratively converged dipole moment was 33D, in good agreement with the experimental available result of 32D. This approach enables us to simulate the effect of the medium polarization upon the electrical properties of asymmetric unit of the crystal surrounded by a sub-field polarization due to other molecules treated as point charges. This polarization procedure is based on the fact that the dominant intermolecular interactions are electrostatic in nature, and also takes into account the long-range electrostatic effects.[27]

In addition to the polarizable π-electrons, the push-pull chromophores requires non-centrosymmetric packing, i.e., space groups lacking inversion center, because all second-order effects can only occur in such space groups.[5] Therefore, suitable second-order NLO materials are those with large first hyperpolarizability values found in molecules that lack an inversion center. As we will see, the 2-amino-chalcone turns out to be centrosymmetric in its crystal form, which hinders their second-order electrical response. However, in liquid phase, the 2-amino-chalcone molecule assumes a non-centrosymmetric conformation making room for second-order NLO applications. As a result, it is important to take into account the solvent effects on liquid 2-amino-chalcone in addition to the crystal environment polarization effects. Many theoretical and experimental investigations reporting the solvent effects are currently carried out in order to evaluate solvent interference in the electronic structure of organic chromophores.[28–30] We selected chloroform, tetrahydrofuran (THF), acetone, ethanol, methanol, dimethyl sulfoxide (DMSO) as well as gas phase to play the role of the surrounding media. For that purpose, we used a continuum solvation model to simulate the solvent influence on the 2-amino-chalcone electronic structure.

Methodology

Synthesis and crystallization. To a solution of 3-bromo-5-hydroxybenzaldeyde (2 mmol) and 2-aminocetophenone (2 mmol) in 8.0 mL of ethanol, an amount of 1.0 mL of 24% sodium hydroxide in water at 10 °C was added. After stirring overnight at room temperature, the solid was filtered, analyzed by ESI-MS and recrystallized from ethanol to afford a crystalline solid. ESI-MS spectrum are show in the supporting information file (Figure S1).

Crystallographic Characterization. The single-crystal X-ray diffraction data for the amino chalcone $C_{15}H_{12}BrNO_2$ were

collected at 120(2) K using a APEX2[31] diffractometer with MoKα radiation (λ=0.71073 Å). The cell refinement and data reduction were carried out also using the software SAINT.[32] The structure (Figure 1) was solved by direct methods using SHELXS[33,34] and anisotropically refined with full-matrix least-squares on F^2 using SHELXL.[35] The hydrogen atoms on the carbon atoms were positioned geometrically and refined using the riding model [C-H 0.93 Å with Uiso(H) = 1.2Ueq(C) for C sp2]. Molecular representation, tables and pictures were generated by WinGX[36], ORTEP-3[36], MERCURY 3.5,[37,38] Mogul[39] and POV-RAY[40] programs. The intermolecular interactions of the title compound were quantified using PARST[41] and PLATON[42,43] programs. The intermolecular contacts in the crystal structure were analyzed using Hirshfeld surfaces[44,45] and the associated 2D fingerprint plots[46] were calculated using Crystal Explorer 3.1 [45]. This approach is a graphical tool used for visualization of intermolecular interactions. The crystallographic data were deposited in the Cambridge Crystallographic Data Centre (deposit@ccdc.camac.uk) under accession number 1432625.

Computational Details. All electronic structure calculations performed in this work were done within Kohn-Sham Density Functional Theory (DFT)[24,25] using the CAM-B3LYP exchange-correlation[47] functional combined with the large 6-311+G(d) Pople split-valence basis set. CAM-B3LYP combines the features of hybrid functionals such as B3LYP[48] with the long-range corrected functionals of Hirao *et al.*,[49] and has been successfully used in the investigation of NLO properties.[50–53]

As already mentioned, the theoretical study developed in this work included the effect of the environment on the NLO properties of 2-amino-chalcone in two ways: (i) effect of solvent and (ii) polarization effect of the crystalline environment. To analyze the effect of solvent on the geometrical and NLO properties of the 2-amino-chalcone, we consider different solvents, especially: chloroform (ε = 4.71), THF (ε = 7.42), acetone (ε = 20.49), ethanol (ε = 24.85), methanol (ε = 32.61) and DMSO (ε = 46.70). These solvents have been used in experimental measurements of the NLO properties of organic compounds.[54–56] Geometry optimization was conducted followed by harmonic frequency calculations to verify whether we have located a genuine minimum or not. To include the solvent in our theoretical calculations, we have employed the self-consistent reaction field (SCRF) approach with the polarizable continuum model (PCM),[57] where the solute molecule is enclosed in a cavity embedded in a dielectric medium.

As commonly used in the literature, the calculated physicochemical properties are here expressed as dipole moment (μ), average linear polarizability (<α>), first-order hyperpolarizability aligned along the dipole moment in "T" convention (β_z^T), and average second-order hyperpolarizability (<γ>), which are orientationally invariant quantities:

$$\mu = \sqrt{\mu_x^2 + \mu_y^2 + \mu_z^2}, \quad (1)$$

$$\langle\alpha\rangle = \frac{\alpha_{xx} + \alpha_{yy} + \alpha_{zz}}{3}, \quad (2)$$

$$\beta_z^T = \beta_{zzz} + \frac{1}{3}\left(\beta_{zxx} + 2\beta_{xzx} + \beta_{zyy} + 2\beta_{yzy}\right) \quad (3)$$

and

$$\langle\gamma\rangle = \frac{1}{15}\sum_{ij=x,y,z}\left(\gamma_{iijj} + \gamma_{ijij} + \gamma_{ijji}\right). \quad (4)$$

We report the often used quantity denoted as $\beta_{||}$, which is given in terms of β_z^T as $\beta_{||} = (3\beta_z^T)/5$. Because the "T" convention is most prevalent in computational quantum chemistry, all hyperpolarizabilities in this work are reported in the "T" notation. For more information about these different notations, the reader should see the references. [52,53]

The particular second and third order NLO processes considered were second harmonic generation (SHG),[58] associated with $\beta_{||}(-2\omega;\omega,\omega)$ and dc-SHG,[59] associated with $\gamma(-2\omega;\omega,\omega,0)$. Frequency-dependent linear polarizabilities $\alpha(-\omega;\omega)$, first order hyperpolarizabilities $\beta_{||}(-2\omega;\omega,\omega)$ and second order hyperpolarizability $\gamma(-2\omega;\omega,\omega,0)$ were computed for the 2-amino-chalcone by using the coupled perturbated (CP)DFT procedure at the characteristic Nd:YAG laser wavelength (λ) of 1064nm (ħω = 0.04282 a.u.).

We also have calculated the dipole moment, linear polarizability and second hyperpolarizability of the asymmetric unit of the 2-amino-chalcone crystal using a hybrid procedure between the supermolecule approach and an iterative electrostatic polarization scheme where the environment polarization effects are attained by assuring the convergence of this molecular properties in the polarization field of surrounding molecules whose atomic sites are treated as point charges. To apply this method, we have used the experimental geometry of the 2-amino-chalcone asymmetric unit as depicted in Figure 1. The crystal packing effects, shown in Figure 2, were modeled considering the nearest nuclear units, 124 asymmetrical units, each with eight molecules treated as point charges, in a 5x5x5 configuration.

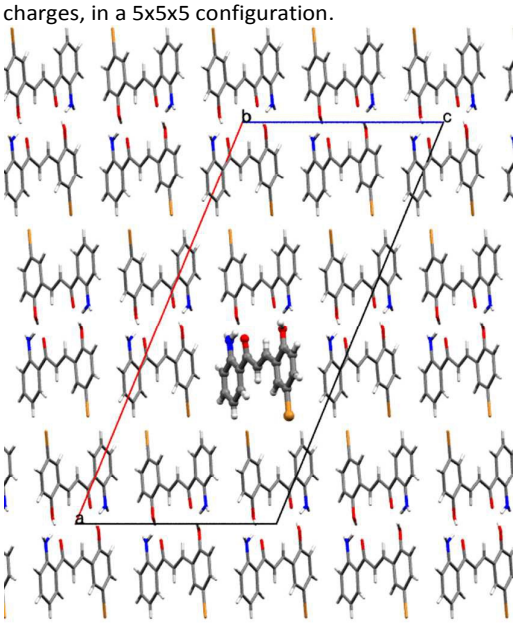

Figure 2. Projection along the b axis of the crystal showing one 2-amino-chalcone ($C_{15}H_{12}BrNO_2$) embedded in the polarization field of the molecules of the surrounding units treated as point charges.

Now we describe a pseudo-code developed for the iterative process of environment polarization effects as follows: (i) perform calculation of partial atomic charges (CHELPG) for the one isolated molecule of the asymmetric unit; (ii) in the position of each corresponding atom in the unit cells generated, to replace the atom by its partial atomic charge, calculated in item (i); (iii) calculate the static electric properties (dipole moment, linear polarizability and second hyperpolarizability), as well as the new partial atomic charges of the asymmetric unit; (iv) return to item (ii) and repeat the procedure until there is convergence in the electric molecular properties. Both geometrical and electronic theoretical calculations were carried out using the Gaussian 09 program suite.[60]

Results and Discussion

Crystallographic structure. The chalcone $C_{15}H_{12}BrNO_2$ crystallizes in monoclinic centrosymmetric space group C2/c with cell parameters a = 29.47(7) Å; b = 6.97(5) Å e c = 13.59(1) Å; β = 112.52(6)°, V = 2581.2(2) Å^3, final *R* indices [I > 2σ(I)] = 0.0178 and goodness-of-fit (*S*) = 1.084. The data relating the final structural refinement, with some information about data collection are shown in Table 1. A strong intramolecular hydrogen bond[61] of type N-H···O [D···A is 2.611(2) Å] is illustrated by dashed lines in ORTEP representation of ellipsoid displacement (Figure 3), which forms a pseudo ring C1– O4 –> O1. The molecule is near to planarity with an angle between the planes of the aromatic rings A and B of 3.08(8)°.

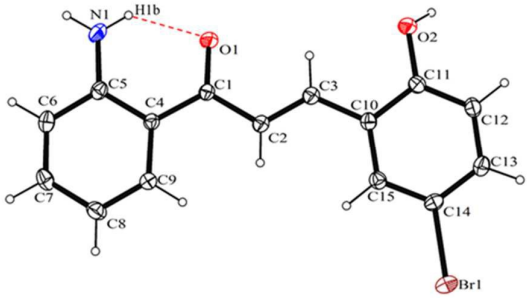

Figure 3. The molecular structure of C15H12BrNO2 with ellipsoids displacement at 50% probability and atomic numbering system. The hydrogen atoms are shown as arbitrary spheres. Dashed lines represent intramolecular hydrogen bond between N1-H1b···O1.

Table 1. Crystal data and refinement parameters of the 2-amino-chalcone $C_{15}H_{12}BrNO_2$

Empirical formula	$C_{15}H_{12}BrNO_2$
Formula weight	318,16 g/mol
Temperature	120(2) K
Wavelength	0.71073 Å
Crystal system	Monoclinic
Space Group	C2/c
Unit cell dimensions	a = 29.47(6) Å b = 6.97(5) Å β = 112.52(6)° c = 13.59(1) Å
Volume	2581.2(1) Å^3
Z	8
Calculated density (g/cm3)	1.637 g/cm^3
Absorption coefficient	3.81 mm^{-1}
F(000)	1280
Crystal size	0.152 x 0.102 x 0.065 mm
θ range for data collection	1.496° to 24.993°
Limiting indices	-34 ≤ h ≤ 34, -8 ≤ k ≤ 8, -16 ≤ l ≤16
Reflections collected	33959
Reflections unique	2275 [R(int) = 0.0223]
Data completeness to θ = 25.242°	97.0%
Data / restrictions / parameters	2275 / 0 / 187
Solution / refinement	Direct methods / least-square full matrix on F^2
S (Goodness-of-fit)	1.084
Final *R* indices [I>2σ(I)]	R1 = 0.0178; wR2 = 0.0460
R indices (All data)	R1 = 0.0194; wR2 = 0.0470
Δρmax. and Δρmin. (e.Å^{-3})	0.282 e -0.208 e.A^{-3}

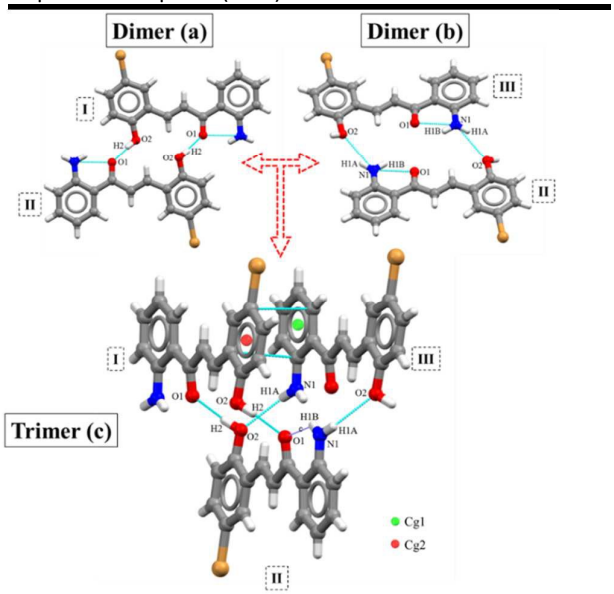

Figure 4. Representation of hydrogen bonds by dashed lines in the dimeric perspective of $C_{15}H_{12}BrNO_2$, involving O2–H2···O1 to dimer (a) and N1–H1A···O2 to dimer (b). Supramolecular arrangement of trimer stabilized by referred hydrogen bonds and π-π stacking between aromatic rings A e B (Cg1 ring A and Cg2 ring B).

The analysis of the geometric parameters in Table 2 was performed using the Mogul program.[39] The statistical results revealed that both bond lengths and bond angles are in

accordance with the expected values. Furthermore, the analysis is able to evaluate that the distances C1=O1 and N1-C5 with 1.245(2) Å; 1.352(2) Å (mean values = 1.239 Å; 1.364 Å) suffer slight variations. The arrangement of the 2-amino-chalcone $C_{15}H_{12}BrNO_2$ leads to hydrogen bonds (Table 3) involving the atoms N1 (donor), O1 (acceptor) also with O2 (donor/acceptor) directly with the conjugate molecules, which combined with the π-π stacking interaction[62] drive a trimeric system. Figure 4 shows the trimer, where molecules I and II interact with each other by O2–H2···O1 [D···A is 2.635(7) Å], while the II and III molecules interact by N1–H1a···O2 [D···A is 3.062(2) Å], and I and III interact by a π-π stacking interaction in parallel zigzag between the aromatic rings (Cg1 and Cg2 are the centroids of the rings A and B) with centroid-centroid distance of 3.686(6) Å, and a displacement between the centroids of 24.1°. Also, the interactions that contribute to stabilize the crystal packing are hydrophobic interactions, especially the π-π and C–H···π contacts (Figure 5). This interaction, also known as hydrogen bond C-H/π (edge-to-face) or also "T interactions",[63] occurs between C6–H6···Cg2 [D···Cg = 3.536(2) Å] and C13–H13···Cg1 [D···Cg = 3.571(2) Å]. These distances are in accordance with what is reported: 3.63 Å, 3.52 Å, 3.80 Å.[64] These interactions, although weak, substantially contribute to the aggregation of molecules within the crystal. It is worth noticing a high complementarity, likewise in the high molecular density in the crystalline arrangement, due to sundry intermolecular interactions that occurred. The C–H···π contacts can aid in a tactile manner to understand aspects of complementarity and the high-density value of 1.637 g/cm^3. The presence of observed intermolecular hydrogen bonds, π-π and C–H···π contacts contribute to stabilize the crystal packing, which explains the ease of obtaining single crystals for this compound, because it is a relatively strong bond type and thus has great influence on the supramolecular arrangement.

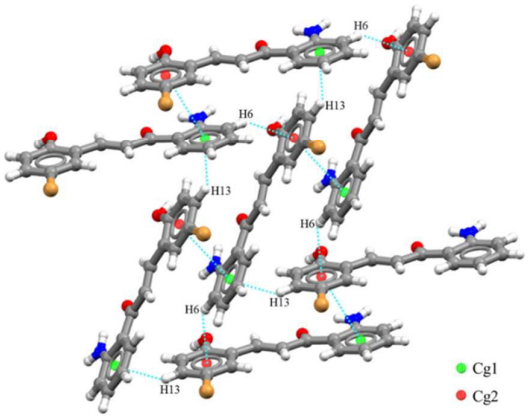

Figure 5. Representation of hydrophobic interactions π–π and C–H···π by dotted lines, establishing a high complementarity to the $C_{15}H_{12}BrNO_2$. Cg1 and Cg2 represents the centroids of aromatic rings A and B. [Symmetry code: Cg1-Cg2 = x,-1+y,z; C13–H13···Cg1 = x,1-y,1/2+z; C6–H6···Cg2 = x,-y,-1/2+z]

Table 2. Bond length and angles, and torsion angles of the $C_{15}H_{12}BrNO_2$. Values in brackets were obtained theoretically at the CAM-B3LYP/6-311+G(d) level in gas phase.

Bond	Value (Å)	Bond	Value (°)	Torsions	Value (°)
C12-C13	1.383(2) [1.385]	C7-C8-C9	119.18(2) [118.722]	C2-C3-C10-C15	-1.4(3) [-20.408]
C7-C6	1.367(2) [1.374]	C8-C7-C6	120.86(2) [120.630]	C10-C3-C2-C1	-176.87(2) [-177.922]
C8-C7	1.388(3) [1.397]	C8-C9-C4	122.33(2) [122.535]	O1-C1-C2-C3	8.4(2) [11.274]
C8-C9	1.366(2) [1.376]	BR1-C14-C13	118.46(1) [119.613]	C3-C2-C1-C4	-171.71(2) [-169.524]
C9-C4	1.413(2) [1.405]	C12-C13-C14	118.89(2) [119.148]	C2-C3-C10-C11	176.37(2) [160.554]
C15-C10	1.398(2) [1.396]	O2-C11-C12	121.50(2) [121.892]	O1-C1-C4-C9	173.68(2) [168.340]
C13-C14	1.382(2) [1.386]	BR1-C14-C15	119.74(1) [119.708]	C9-C4-C1-C2	-6.2(2) [-12.479]
O2-C11	1.360(2) [1.359]	C13-C12-C11	120.29(2) [120.513]	O1-C1-C4-C5	-5.6(2) [-10.343]
BR1-C14	1.898(9) [1.903]	C13-C14-C15	120.80(2) [120.675]	C5-C4-C1-C2	174.57(1) [168.837]
C12-C11	1.386(2) [1.389]	O2-C11-C10	117.79(1) [117.407]		
C15-C14	1.372(2) [1.381]	C10-C15-C14	119.97(2) [121.010]		
C2-C3	1.324(2) [1.335]	C12-C11-C10	120.70(2) [120.698]		
O1-C1	1.245(2) [1.228]	C6-C5-N1	118.78(2) [119.134]		
C10-C11	1.403(2) [1.402]	C7-C6-C5	121.35(2) [121.3914]		
C5-N1	1.352(2) [1.358]	O1-C1-C2	118.89(1) [118.991]		
C10-C3	1.458(2) [1.464]	C3-C2-C1	121.46(2) [120.094]		
C6-C5	1.407(2) [1.409]	C15-C10-C11	118.32(2) [117.951]		
C2-C1	1.474(2) [1.487]	C15-C10-C3	122.69(2) [122.581]		
C4-C5	1.425(2) [1.422]	C10-C3-C2	127.55(2) [126.030]		
C4-C1	1.456(2) [1.476]	C4-C5-N1	122.77(2) [122.371]		
		C6-C5-C4	118.45(2) [118.481]		
		C9-C4-C5	117.84(1) [118.214]		
		O1-C1-C4	120.37(2) [121.557]		
		C9-C4-C1	121.11(1) [121.221]		
		C4-C1-C2	120.74(2) [119.447]		
		C11-C10-C3	118.96(2) [119.461]		
		C5-C4-C1	121.05(1) [120.553]		

New Journal of Chemistry

ARTICLE

Table 3. Hydrogen bonds and C–H···π interactions of $C_{15}H_{12}BrNO_2$[a]

Type	D–H···A	D–H (Å)	H···A (Å)	D···A (Å)	D–H···A (°)
Inter	N1–H1a···O2[i]	0.82(2)	2.33(2)	3.062(2)	149.4(2)
Intra	N1–H1b···O1	0.83(2)	1.97(2)	2.611(2)	133.4(2)
Inter	O2–H2···O1[ii]	0.79(2)	1.85(2)	2.635(7)	173.(2)
Inter	C6–H6···Cg2[iii]	0.91(2)	2.78(2)	3.536(2)	141.3(2)
Inter	C13–13···Cg1[iv]	0.92(2)	2.75(2)	3.571(2)	148.2(2)

[a][Symmetry code: i = -x,-y,-z; ii = -x,-y+1,-z; iii = x,-y,-1/2+z; iv = x,1-y,1/2+z].

Hirshfeld surface analysis. Throughout Crystal Explorer 3.1 program [45], the Hirshfeld surfaces graphics were obtained as an additional methodology for the study of intermolecular interactions in order to confirm the occurrence region of the hydrogen bond, π-π and C–H···π contacts. Figure 6 shows the structure of the title compound that prevails weaker contacts located around the hydrophobic regions of the molecules, surrounding carbon and hydrogen atoms (in blue). Furthermore, a small portion of contacts (in red) takes place mostly around the carbonyl, hydroxyl and amino groups. These chemical groups participate in intermolecular interactions. The fingerprint plot tool appears to be more informative in terms of contacts between atoms. The graph is constructed by a projection of d_e (ordinate - distance from the surface to the nearest atom exterior to the surface) against d_i (abscissa - distance from the surface to the nearest atom interior to the surface).[46] Figure 7 shows the fingerprint plot, detailing the percentage at which that each meaningful contact occurs, including a plot of all contacts (Figure 7A). The intermolecular contacts that can be explored from this structure are: C···H, O···H, C···C, H···H, Br···H, O···O, C···O, Br···Br, Br···C, C···N, N···H and O···N. The H···O contacts (Figure 7C) that can be observed are located in the lower limits of de and di, and have a form like a fine and elongated trace. The compounds, which exhibit this elongated trace, typically show a classic intermolecular hydrogen bond. The remaining H···O contacts are in the top regions of the plot and are inherent with weak interactions (non-classical hydrogen bonds).

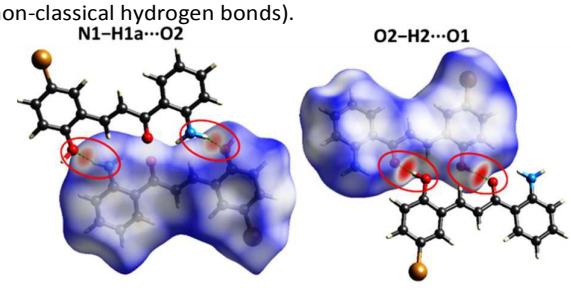

Figure 6. Hirshfeld surface mapped with d_{norm} mapped on Hirshfeld surface for visualizing the intercontacts. Dashed lines represent hydrogen bonds between N1–H1a···O2 and N1–H1b···O1, in red color regions.

The final approach about π-π interactions was done using the Hirshfeld surface shape index. On this surface, the π-π interactions can be identified by combining two complementary triangular patches.[65] Figure 8 shows the shape index surface, obtained for the title compound in two different perspectives of view, which there are highlighted triangles patches formed on each side, where blue regions are in contact with the regions in red of the neighboring molecule and vice versa. It is observed that at least one side of the molecule centroid participates in the π-π interactions. This is an indication of the formation of a chain united by this kind of interaction. On the surface, only triangles in Cg1 are formed at the top, while the triangles in Cg2 are not well formed and contrary to the surface below. This supports the hypothesis that π-π interactions in this structure can contribute to the formation of dimer. However, it is noted that dimer formation was observed mainly due the hydrogen bonds previously discussed, though this does not eliminate the possibility that the π–π interactions contribute to the supramolecular arrangement described.

Conventionally, the hydrophobic interactions are marked by contacts between C···C, C···H and H···H, and these are not easily observed or measured, especially the last two. However, with the fingerprint plot, these interactions can be observed in a generic way. The contacts C···H (Figure 7B) are mainly located at regions near the A and B aromatic rings with the carbon atoms of the system. By fingerprint, the highlighted contact is between hydrogen atoms H···H (Figure 7E). In this structure, although the bromine atoms do not involve any traditional intermolecular interaction, they presented a considerable percentage of Br···H contacts (Figure 7F), probably due to their van de Waals radius being relatively large compared to the other atoms. This is in a region close to the C···H contacts, because the bromine are covalently bonded to the aromatic ring B. The contacts between carbon atoms (C···C) is not extensive, but assumes a great deal of importance, because it is related to the π-π interaction which has been discussed. The main characteristic of C···C contacts is about the distribution of contact points in a centric area of the mapped color plot, which is similar to a triangle form as shown in Figure 7D. This mainly indicates the formation of π-π interactions, because these interactions occur between rigid bodies, so their distances do not suffer many variations. This type of interaction has some peculiarities already discussed.

Computational studies. To assess the NLO response of the 2-amino-chalcone in terms of the electric properties that generate the microscopic NLO quantities, we have performed quantum chemical calculations using the CAM-B3LYP/6-311+G(d) level of theory using two approaches: (i) taking into account the packing effects (embedded partial atomic charges) through an iterative procedure; and (ii) considering the title compound in different solvent media. We begin our discussion

with the former procedure, where the applicability of this electrostatic embedding approach relies on the fast convergence of the electric properties of the crystal during the iterative process of electric polarization (see Figure 9), which begins with the atomic charge of isolated 2-amino-chalcone. The results of the approximation CAM-B3LYP/6-311+G(d) for the linear polarizability and second hyperpolarizability, obtained for isolated chalcone and converged in the presence of incorporated charges, are shown in Table 4. These results stand for the dynamic calculations of α and γ using a polarizing radiation of frequency ω = 0.0428 a.u. (λ = 1064nm). Clearly, one can notice from Table 4 that γ(-2ω;ω,ω,0) is much more sensitive to the inclusion of 2-amino-chalcone in the crystal lattice with an increase of almost 20% when we compare the isolated with the embedded form, whereas for α(-ω;ω), the increase is almost negligible. The geometry used for such calculations was obtained from experimental X-ray diffraction represented in Table 2, without any further full geometrical optimization.

Table 4. CAM-B3LYP/6-311+G(d) results for the dynamic linear polarizability (in 10-24 esu) and second hyperpolarizability (in 10^{-36} esu) of isolated and embedded 2-amino-chalcone for the frequency $\omega = 0.0428$ a.u.

	α(-ω;ω)	γ(-2ω;ω,ω,0)
Isolated	33.34	120.74
Embedded	33.89	144.12

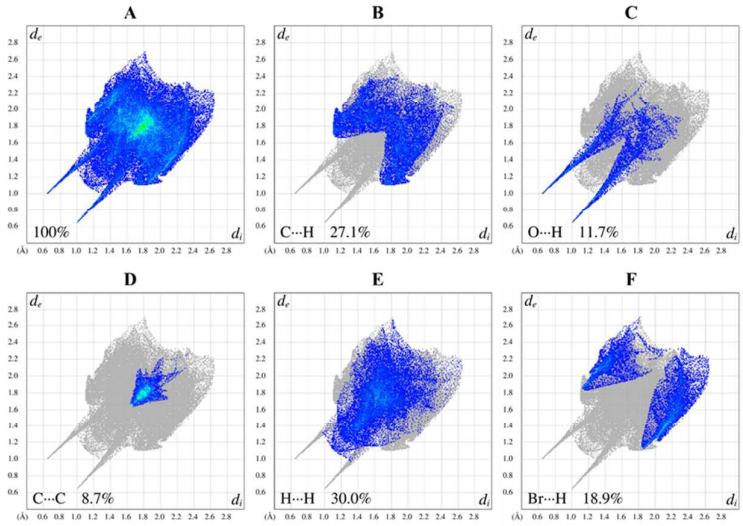

Figure 7. The Fingerprint plot for the title compound: A) 100% of contacts; B) C···H; C) O···H; D) C···C; E) H···H and F) Br···H. Produced from d_e and d_i function mapped in color showing the percentage contribution of each type of interaction in total interactions verified. d_e - distance from the surface to the nearest atom exterior to the surface) against d_i - distance from the surface to the nearest atom interior to the surface).

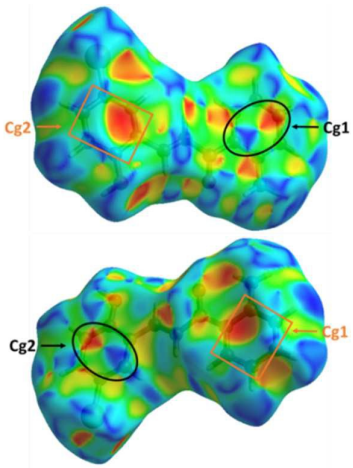

Figure 8. Shape index Hirshfeld surface of $C_{15}H_{12}BrNO_2$, showing the complementary patches where π–π interactions occur. Highlighted regions indicate complementary patches (black ellipses with one another are self-complementary and orange rectangles do not show π–π interactions).

One of the reasons for the γ growth (and to a lesser extent for μ and α) in a crystalline environment can be found analysing the results summarized in Table S3, where the CHELPG atomic charges from the iterative procedure are depicted in detail. Observing these results, there is a significant charge transfer from donor groups to the bromine atom (electron acceptor) when we compare the isolated (iteration 0) with the [converged] (iteration 5) embedded 2-amino-chalcone. We can see this by verifying that the net charge of the amino group (NH3) has decreased 49.76% (-0.10218e [-0.05085e]). On the other hand, the bromine atomic charge has increased 39.70% (-0.11112e [-0.15524e]). Thereby, the packing effects on the asymmetric electron's distribution is to increase the NLO quantities for this molecular system. Following the discussion in the crystallographic structure section, 2-amino-chalcone crystalizes in a centrosymmetric lattice. Nevertheless, regarding the second hyperpolarizability γ(-2ω;ω,ω,0), there are no symmetry requirements for the observation of a third order nonlinear response.[5] The synthesized title compound is a potential candidate for third order NLO applications due to their high crystallinity and relatively large γ(-2ω;ω,ω,0), which is microscopically related to dc-induced second harmonic

generation.[59] Our result for the embedded form of 2-amino-chalcone γ(-2ω;ω,ω,0) = 144.12×10^{-36} esu is comparable to the experimental results of other organic chromophores such as stilbene derivatives.[66]

In addition to the dynamic calculations, we have performed iterative computation for the static case (ω = 0) using the same pseudo-code of embedded point charges. In Figure 9, we present the convergence of the aimed quantities as a function of the number of iteration steps. To avoid the proliferation of tables and figures we present the results for the static case in the Supporting Information section, except for the Figure 9. From Figure 9, one can notice that a fast convergence is reached at the fifth iteration for all electric properties. The dipole moment converges to 2.03D for the embedded 2-amino-chalcone, revealing that the polarization effects contribute to an increase of 46% compared with the result of isolated 2-amino-chalcone. The results for the other properties iteration-by-iteration are summarized in Table S1. The static linear polarizability <α> converged to 32.86.10^{-24} esu (an increase less than 2%), while the converged static second hyperpolarizability has also increased, although just 8% with respect to the isolated form. (The increase was 20% for dynamic calculations.) When confronting the dynamic with the static results, we notice that the most significant differences lie in the second hyperpolarizability, as can be verified in Table 4 and S1, γ(-2ω;ω,ω,0) = 144.12 and <γ> = 69.29 (both in 10^{-36} esu units).

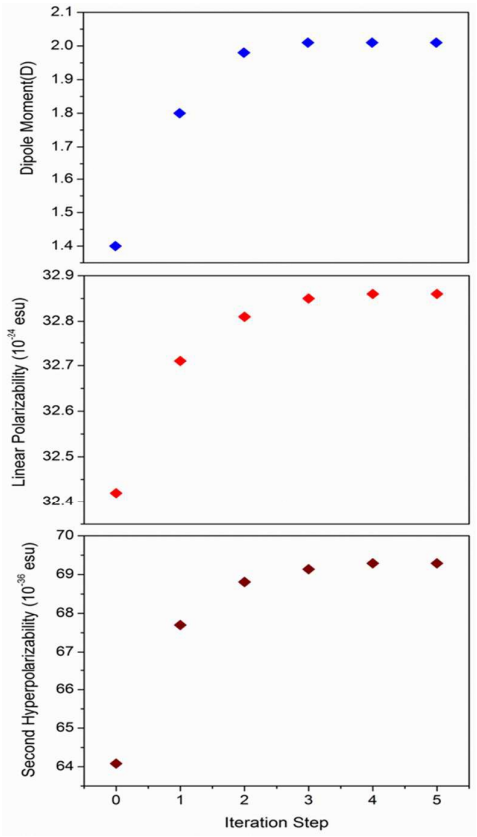

Figure 9. Evolution of the calculated values of the dipole moment, linear polarizability and second hyperpolarizability of 2-amino-chalcone with respect to the number of iterations.

We have also calculated the dynamic electric properties of the 2-amino-chalcone, but this time by including different solvents (gas, chloroform, tetrahydrofuran, acetone, ethanol, methanol and dimethyl sulfoxide), because the 2-amino-chalcone molecule assumes a non-centrosymmetric conformation in solution, so that the first hyperpolarizability does not vanish using an implicit solvation scheme based on the integral equation formalism of PCM (IEF-PCM). The results for the extreme cases, i.e., gas phase and dimethyl sulfoxide, are presented in Table 5, showing the linear polarizability as well as first and second hyperpolarizability. Just like for the embedded case discussed in Table 4, the γ(-2ω;ω,ω,0) values are much more sensitive to the presence of polar solvents than are β//(-2ω;ω,ω) and α(-ω;ω) values. We can confirm this in terms of figures verifying that DMSO has increased by almost 96% the γ(-2ω;ω,ω,0) values, whereas for β//(-2ω;ω,ω) and α(-ω;ω), the increase was 52% and 14%, respectively.

Table 5. CAM-B3LYP/6-311+G(d) results for the dynamic linear polarizability (in 10^{-24} esu), first hyperpolarizability (in 10^{-30} esu) and second hyperpolarizability (in 10^{-36} esu) of gas-phase and DMSO solvent 2-amino-chalcone for the frequency $\omega = 0.0428$ a.u.

Medium	α(-ω;ω)	β||(-2ω;ω,ω)	γ(-2ω;ω,ω,0)
Gas-Phase	34.87	3.05	132.90
DMSO	39.68	4.64	260.163

The geometry used for the calculations of NLO properties of solvated 2-amino-chalcone was optimized via the CAM-B3LYP/6-311+G(d) level of calculation and the geometrical parameters of the optimized structure in gas-phase are presented in brackets in Table 2. We can notice that the most important discrepancies between the experimental and theoretical results are those of dihedral angles due to the environment packing effects. The observations made for the dynamic calculations were a general trend for the static case as well. In Table S2 are presented the dipole moment μ, static linear polarizability <α>, first hyperpolarizability β// and second hyperpolarizability <γ> results, obtained via the CAM-B3LYP/6-311+G(d) level of calculation. The increase of each property due to the inclusion of DMSO as the surrounding medium, for instance, was 39%, 36% and 171% for, μ, <α> and <γ>, respectively, demonstrating the capacity of polar solvents to stabilize dipolar species, eventually leading to a higher nonlinear response.[30] This increase of the NLO properties are closely related to the intramolecular charge transfer due to the mesomeric effects impelled by the D-A groups capped at opposite sides within the molecular system. In Table S4, the CAM-B3LYP/6-311+G(d) results for the CHELPG atomic charges are presented and we can see that the relative polarity of the medium does affect the intramolecular charge transfer. A significant redistribution of charge density takes place as we increase the solvent dielectric constant. Our results give that the solvated [gas phase] bromine atom (electron acceptor) has a partial charge of -0.125212e [-0.109761e] in DMSO, whereas the amino group (electron donor) has a net charge of -0.162304e [-0.178349e], indicating a charge depletion of the electron-donating amino group and a charge increase of the electron-acceptor bromine atom when in DMSO. These results corroborate to the asymmetric electronic density's distribution giving rise to larger vales of $\beta_{//}$ and <γ> as the solvent polarity increases. However, as a consequence of the 2-amino-chalcone crystal structure, which is a monoclinic

centrosymmetric space group C2/c, second order applications for this molecule are suppressed in solid state. On the other hand, the solvated form is a potential NLO candidate as a result of its non-centrosymmetric molecular arrangement, push-pull induced mesomeric effects and intramolecular charge transfer. Our results show a relatively low value for $\beta_{//}(-2\omega;\omega,\omega)$ (4.64×10^{-30} in DMSO), especially when we compare it to the experimental value for p-nitro aniline (a common prototype for NLO applications) in DMSO (28.8×10^{-30} esu).[67] Despite the fact that this result might seem to be a drawback, our results for the second hyperpolarizability puts forth 2-amino-chalcone as an interesting system for third order nonlinear applications.

Conclusions

A new chalcone derivative has been synthesized with an amino group as an electron-donating functional group and a bromine atom as electron-acceptor. The title compound crystallized in a centrosymmetric monoclinic centrosymmetric space group C2/c with cell parameters a = 29.47(7) Å; b = 6.97(5) Å e c = 13.59(1) Å; β = 112.52(6)°, V = 2581.2(2) $Å^3$, final R indices [I > 2σ(I)] = 0.0178 and goodness-of-fit (S) = 1.084. The molecule is near to planarity, with an angle between the planes of the aromatic rings A and B of 3.08(8)°. The formation of dimers was verified analysing Hirshfeld surfaces in order to confirm the occurrence of regions with hydrogen bond, π-π and C–H···π contacts. We observed that the dimer shows a classic intermolecular hydrogen bond and that at least one side of the molecule centroid participates in the π-π interactions, indicating the formation of a chain united by this kind of interaction, endorsing the existence of a dimer arrangement. Being a D-A molecular system, we have investigated the NLO properties of the asymmetric unit of 2-amino-chalcone using the CAM-B3LYP/6-311+G(d) level of theory. The dipole moment, linear polarizability and second hyperpolarizability have been evaluated by means of a supermolecular approach in combination with an iterative electrostatic interaction approximation in which the surrounding molecules within the unit cell are represented by their respective atomic charges. Rapid convergence of the electric properties was attained, indicating that this approach is feasible for the description of electric properties in organic crystals. Our results showed that $\gamma(-2\omega;\omega,\omega,0)$ is much more sensitive to the inclusion of 2-amino-chalcone in the crystal lattice with an increase of almost 20% when we compare the isolated with the embedded form, whereas for $\alpha(-\omega;\omega)$, the increase is almost negligible. The final result for the embedded form of 2-amino-chalcone $\gamma(-2\omega;\omega,\omega,0)$ = 144.12×10^{-36} esu is comparable to the experimental results of other organic chromophores.

Dynamic and static electric properties of the 2-amino-chalcone in different solvent media is reported because the title compound assumes a non-centrosymmetric conformation in solution, so $\beta_{//}(-2\omega;\omega,\omega)$ does not vanish. The solvent DMSO has augmented almost 96% the $\gamma(-2\omega;\omega,\omega,0)$ values whereas for $\beta_{//}(-2\omega;\omega,\omega)$ and $\alpha(-\omega;\omega)$, the augmentation was 52% and 14%, respectively, when comparing it with the free-solvent situation. CHELPG atomic charges indicated there is a significant charge transfer from donor groups to the bromine atom, where the net charge of the amino group (NH_3) has decreased 49.76% and bromine atomic charge has increased 39.70% for the converged in-crystal situation. We found a relatively low value for $\beta_{//}(-2\omega;\omega,\omega) = 4.64\times10^{-30}$ esu in DMSO. However, the second hyperpolarizability results indicate that the 2-amino-chalcone is an interesting system for third order nonlinear applications.

Acknowledgements

The authors would like to thank the following Brazilian agencies for financial support: Conselho Nacional de Desenvolvimento Científico e Tecnológico (CNPq), Coordenação de Aperfeiçoamento Pessoal de Nível Superior (CAPES) and Fundação de Apoio à Pesquisa do Distrito Federal (FAP-DF). The authors also thank the organizers of the 2014 ACA Summer Course for Chemical Crystallography for single-crystal X-ray diffraction data collection.

Notes and references

‡ Footnotes relating to the main text should appear here. These might include comments relevant to but not central to the matter under discussion, limited experimental and spectral data, and crystallographic data.

1 S. M. A. Davydov B.L., Derkacheva L.D., Dunina V.V., Zhabotinskii M.E., Zolin V.F., Koreneva L.G., *JEPT Lett.*, 1970, **12**, 24–26.

2 J. Indira, P. P. Karat and B. . Sarojini, *J. Cryst. Growth*, 2002, **242**, 209–214.

3 E. D. D'silva, G. K. Podagatlapalli, S. V. Rao, D. N. Rao and S. M. Dharmaprakash, *Cryst. Growth Des.*, 2011, **11**, 5362–5369.

4 C. S. Chidan Kumar, S. Raghavendra, T. S. Chia, S. Chandraju, S. M. Dharmaprakash, H.-K. Fun and C. K. Quah, *Opt. Mater. (Amst).*, 2015, **49**, 279–285.

5 P. Günter, *Nonlinear Optical Effects and Materials*, Springer Berlin Heidelberg, Berlin, 4th edn., 2000.

6 T. L. Fonseca, H. C. B. De Oliveira, O. A. V Amaral and M. A. Castro, *Chem. Phys. Lett.*, 2005, **413**, 356–361.

7 T. L. Fonseca, M. A. Castro, H. C. B. de Oliveira and S. Cunha, *Chem. Phys. Lett.*, 2007, **442**, 259–264.

8 H. C. B. de Oliveira, T. L. Fonseca, M. A. Castro, O. A. V. Amaral and S. Cunha, *J. Chem. Phys.*, 2003, **119**, 8417.

9 D. Jacquemin, *J. Phys. Chem. A*, 2004, **108**, 9260–9266.

10 N. V Agrinskaya, V. A. Lukoshkin, V. V Kudryavtsev, G. I. Nosova, N. A. Solovskaya and A. V Yakimanskii, *Phys. Solid State*, 1999, **41**, 1914–1917.

11 B. Ganapayya, A. Jayarama and S. M. Dharmaprakash, *Mol. Cryst. Liq. Cryst.*, 2013, **571**, 87–98.

12 J. Wu, C. Wang, Y. Cai, J. Peng, D. Liang, Y. Zhao, S. Yang, X. Li, X. Wu and G. Liang, *Med. Chem. Res.*, 2012, **21**, 444–452.

13 Y. K. Rao, S.-H. Fang and Y.-M. Tzeng, *Bioorg. Med. Chem.*, 2009, **17**, 7909–14.

14 B.-T. Yin, C.-Y. Yan, X.-M. Peng, S.-L. Zhang, S. Rasheed, R.-X. Geng and C.-H. Zhou, *Eur. J. Med. Chem.*, 2014, **71**, 148–59.

15 Z. Liu, L. Tang, P. Zou, Y. Zhang, Z. Wang, Q. Fang, L. Jiang, G. Chen, Z. Xu, H. Zhang and G. Liang, *Eur. J. Med. Chem.*, 2014, **74**, 671–82.

16 B. Kupcewicz, A. A. Jarzęcki, M. Małecka, U. Krajewska and M. Rozalski, *Bioorg. Med. Chem. Lett.*, 2014, **24**, 4260–5.

17 S. Shenvi, K. Kumar, K. S. Hatti, K. Rijesh, L. Diwakar and G. C. Reddy, *Eur. J. Med. Chem.*, 2013, **62**, 435–42.

18 R. Shivahare, V. Korthikunta, H. Chandasana, M. K. Suthar, P. Agnihotri, P. Vishwakarma, T. K. Chaitanya, P. Kancharla, T. Khaliq, S. Gupta, R. S. Bhatta, J. V. Pratap, J. K. Saxena, S. Gupta and N. Tadigoppula, *J. Med. Chem.*, 2014, **57**, 3342–3357.

19 R. Abonia, P. Cuervo, J. Castillo, B. Insuasty, J. Quiroga, M. Nogueras and J. Cobo, *Tetrahedron Lett.*, 2008, **49**, 5028–5031.

20 J. A. Donnelly and D. F. Farrell, *J. Org. Chem.*, 1990, **55**, 1757–1761.

21 W. A. Silva, C. C. Gatto and G. R. Oliveira, *Acta Crystallogr. Sect. E. Struct. Rep. Online*, 2011, **67**, o2210.

22 G. de Oliveira, H. de Oliveira, W. Silva, V. da Silva, J. Sabino and F. Martins, *Struct. Chem.*, 2012, **23**, 1667–1676.

23 H. G. O. Alvim, E. L. Fagg, A. L. de Oliveira, H. C. B. de Oliveira, S. M. Freitas, M. A. E. Xavier, T. A. Soares, A. F. Gomes, F. C. Gozzo, W. A. Silva and B. A. D. Neto, *Org. Biomol. Chem.*, 2013, **11**, 4764–4777.

24 W. Kohn and L. J. Sham, *Phys. Rev.*, 1965, **137**.

25 P. Hohenberg and W. Kohn, *Phys. Rev.*, 1964, **136**, B864–B871.

26 M. de Wergifosse, F. Castet and B. Champagne, *J. Chem. Phys.*, 2015, **142**, 194102.

27 T. L. Fonseca, J. R. Sabino, M. A. Castro and H. C. Georg, *J. Chem. Phys.*, 2010, **133**, -.

28 R. Misra and S. Kar, *Chem. Phys.*, 2012, **397**, 65–73.

29 R. Misra, A. Mandal, M. Mukhopadhyay, D. K. Maity and S. P. Bhattacharyya, *J. Phys. Chem. B*, 2009, **113**, 10779–10791.

30 T. Jaunet-Lahary, A. Chantzis, K. J. Chen, A. D. Laurent and D. Jacquemin, *J. Phys. Chem. C*, 2014, **118**, 28831–28841.

31 Bruker. APEX2. Bruker AXS Inc., Madison, Wisconsin, USA, 2007.

32 Bruker. SAINT. Bruker AXS Inc., Madison, Wisconsin, USA, 2007.

33 G. M. Sheldrick, *Acta Crystallogr. Sect. A*, 1990, **46**, 467–473.

34 G. M. Sheldrick, *Acta Crystallogr. Sect. A*, 2008, **64**, 112–122.

35 G. M. Sheldrick, *Acta Crystallogr. Sect. C*, 2015, **71**, 3–8.

36 L. J. Farrugia, *J. Appl. Crystallogr.*, 2012, **45**, 849–854.

37 C. F. Macrae, P. R. Edgington, P. McCabe, E. Pidcock, G. P. Shields, R. Taylor, M. Towler and J. van de Streek, *J. Appl. Crystallogr.*, 2006, **39**, 453–457.

38 C. F. Macrae, I. J. Bruno, J. A. Chisholm, P. R. Edgington, P. McCabe, E. Pidcock, L. Rodriguez-Monge, R. Taylor, J. van de Streek and P. A. Wood, *J. Appl. Crystallogr.*, 2008, **41**, 466–470.

39 I. J. Bruno, J. C. Cole, M. Kessler, J. Luo, W. D. S. Motherwell, L. H. Purkis, B. R. Smith, R. Taylor, R. I. Cooper, S. E. Harris and A. G. Orpen, *J. Chem. Inf. Comput. Sci.*, 2004, **44**, 2133–2144.

40 C. J. Cason, POV-RAY. Persistence of Vision Raytracer Pty. Ltd, Victoria, Australia, 2003.

41 M. Nardelli, *J. Appl. Crystallogr.*, 1995, **28**, 659.

42 A. L. Spek, *Acta Crystallogr. Sect. D Biol. Crystallogr.*, 2009, **65**, 148–155.

43 A. L. Spek, *J. Appl. Crystallogr.*, 2003, **36**, 7–13.

44 M. A. Spackman and D. Jayatilaka, *CrystEngComm*, 2009, **11**, 19–32.

45 S. K. Wolff, D. J. Grimwood, J. J. McKinnon, M. J. Turner, D. Jayatilaka and M. A. Spackman, 2012.

46 M. A. Spackman and J. J. McKinnon, *CrystEngComm*, 2002, **4**, 378–392.

47 T. Yanai, D. P. Tew and N. C. Handy, *Chem. Phys. Lett.*, 2004, **393**, 51–57.

48 A. D. Becke, *J. Chem. Phys.*, 1993, **98**, 1372–1377.

49 H. Iikura, T. Tsuneda, T. Yanai and K. Hirao, *J. Chem. Phys.*, 2001, **115**, 3540.

50 N. A. Murugan, J. Kongsted, Rinkevicius and H. Agren, *Proc. Natl. Acad. Sci. United States Am.*, 2010, **107**, 16453–16458.

51 P. Krawczyk, *J. Mol. Model.*, 2010, **16**, 659–668.

52 A. J. Garza, O. I. Osman, A. M. Asiri and G. E. Scuseria, *J. Phys. Chem. B*, 2015, **119**, 1202–1212.

53 A. J. Garza, N. A. Wazzan, A. M. Asiri and G. E. Scuseria, *J. Phys. Chem. A*, 2014, **118**, 11787–11796.

54 L. A. Gómez, C. B. de Araújo, A. M. Brito-Silva and A. Galembeck, *Appl. Phys. B*, 2008, **92**, 61–66.

55 L. de M. Furtado and L. Gómez-Malagón, *Plasmonics*, 2014, **9**, 1377–1389.

56 M. Pannipara, A. Asiri, K. Alamry, I. Salem and S. El-Daly, *J. Fluoresc.*, 2015, **25**, 103–112.

57 B. Mennucci, *Wiley Interdiscip. Rev. Comput. Mol. Sci.*, 2012, **2**, 386–404.

58 D. R. Kanis, M. A. Ratner and T. J. Marks, *Chem. Rev.*, 1994, **94**, 195–242.

59 D. M. Bishop, in *Advances in Chemical Physics*, John Wiley & Sons, Inc., 1998, pp. 1–40.

60 M. J. Frisch, G. W. Trucks, H. B. Schlegel, G. E. Scuseria, M. A. Robb, J. R. Cheeseman, G. Scalmani, V. Barone, B. Mennucci, G. A. Petersson, H. Nakatsuji, M. Caricato, X. Li, H. P. Hratchian, A. F. Izmaylov, J. Bloino, G. Zheng, J. L. Sonnenberg, M. Hada, M. Ehara, K. Toyota, R. Fukuda, J. Hasegawa, M. Ishida, T. Nakajima, Y. Honda, O. Kitao, H. Nakai, T. Vreven, J. A. Montgomery, J. E. Peralta, F. Ogliaro, M. Bearpark, J. J. Heyd, E. Brothers, K. N. Kudin, V. N. Staroverov, R. Kobayashi, J. Normand, K. Raghavachari, A. Rendell, J. C. Burant, S. S. Iyengar, J. Tomasi, M. Cossi, N. Rega, J. M. Millam, M. Klene, J. E. Knox, J. B. Cross, V. Bakken, C. Adamo, J. Jaramillo, R. Gomperts, R. E. Stratmann, O. Yazyev, A. J. Austin, R. Cammi, C. Pomelli, J. W. Ochterski, R. L. Martin, K. Morokuma, V. G. Zakrzewski, G. A. Voth, P. Salvador, J. J. Dannenberg, S. Dapprich, A. D. Daniels, Farkas, J. B. Foresman, J. V Ortiz, J. Cioslowski and D. J. Fox, *Gaussian 09, Revis. D.01, Gaussian, Inc., Wallingford CT*, 2009.

61 G. R. Desiraju and T. Steiner, *The Weak Hydrogen Bond: In Structural Chemistry and Biology*, Oxford University Press, 2001.

62 C. A. Hunter and J. K. M. Sanders, *J. Am. Chem. Soc.*, 1990, **112**, 5525–5534.

63 J. Tiekink, E. R. T.; Schpector-Zukerman, in *The Importance of Pi-Interactions in Crystal Engineering*, John Wiley & Sons, Ltd, 2012, pp. c1–c8.

64 T. Kobkeatthawin, S. Chantrapromma, C. S. Chidan Kumar and H.-K. Fun, *Acta Crystallogr. Sect. E Struct. Reports Online*, 2013, **69**, o1750–o1751.

65 J. J. McKinnon, M. A. Spackman and A. S. Mitchell, *Acta Crystallogr. Sect. B*, 2004, **60**, 627–668.

66 U. Gubler, S. Concilio, C. Bosshard, I. Biaggio, P. Günter, R. E. Martin, M. J. Edelmann, J. A. Wytko and F. Diederich, *Appl. Phys. Lett.*, 2002, **81**, 2322.

67 J. N. Woodford, M. A. Pauley and C. H. Wang, *J. Phys. Chem. A*, 1997, **101**, 1989–1992.

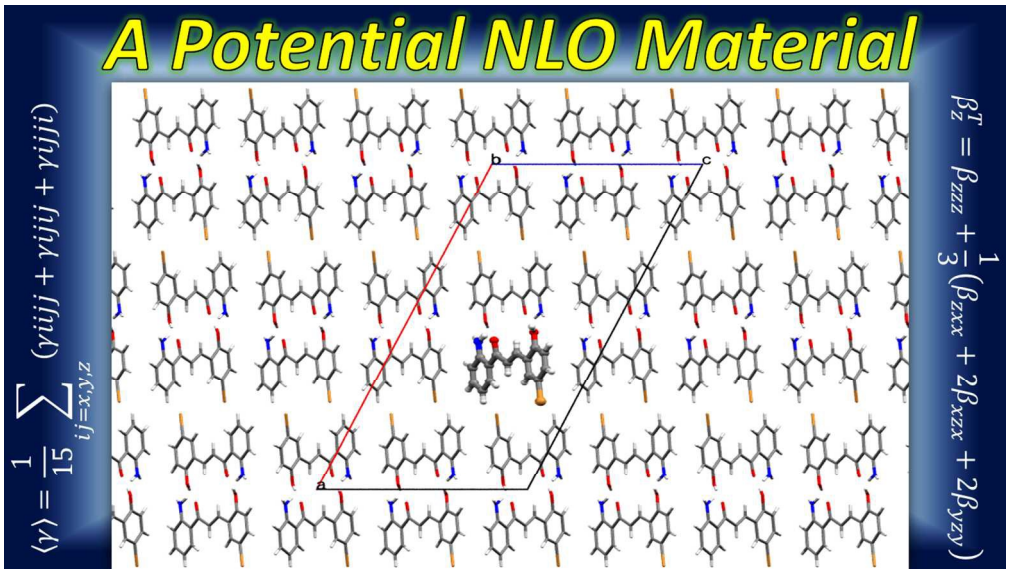

243x137mm (150 x 150 DPI)